Supporting Information

Flexible control of Co/Zn-nitrogen coordination in ZIFs for electrochemical CO_2 reduction to tunable syngas

Yanjun Liu and Ning Yuan*

School of Chemical and Environmental Engineering, China University of Mining and Technology, Beijing 100083, China

*Corresponding Author: Ning Yuan, E-mail address: ning.yuan@cumtb.edu.cn

Materials and methods

Materials

$Co(NO_3)_2 \cdot 6H_2O$ was purchased from Beijing Shuanghuan Chemical Reagent Factory, 2-methylimidazole was purchased from Shanghai Titan Technology Co., Ltd., $Zn(NO_3)_2 \cdot 6H_2O$ was purchased from Shanghai Aladdin Biochemical Technology Co., Ltd., and anhydrous methanol was purchased from Beijing Modern Oriental Fine Chemical Co., Ltd. All solvents can be used without further purification.

Synthesis of catalyst

$Zn(NO_3)_2 \cdot 6H_2O$ was combined with $Co(NO_3)_2 \cdot 6H_2O$ in 7.5 mL of methanol, with amounts of 1.0, 0.75, 0.5, 0.25 and 0 mmol for $Zn(NO_3)_2 \cdot 6H_2O$ and 0, 0.25, 0.5, 0.75 and 1.0 mmol for $Co(NO_3)_2 \cdot 6H_2O$. Then, 3.64 mmol of 2-methylimidazole was dissolved in 7.5 mL of methanol and quickly poured into the above solution while stirring at room temperature for 10 hours to prepare Co_0Zn_1-ZIF, $Co_{0.25}Zn_{0.75}$-ZIF, $Co_{0.5}Zn_{0.5}$-ZIF, Co_1Zn_0-ZIF and $Co_{0.75}Zn_{0.25}$-ZIF, respectively. The resulting precipitate was centrifuged, washed three times with methanol, and dried overnight at 80 °C.

Catalyst characterization methods

The surface morphology and size of the sample before and after electrocatalysis were analyzed using a scanning electron microscope (SEM) (ZEISS Gemini 300). The corresponding elemental distribution map was obtained using an energy-dispersive spectrometer (EDS) (OXFORD XPLORE30). Fine structural analysis was performed using a scanning transmission electron microscope (STEM) (JEM-2100F). X-ray diffraction (XRD) data were collected using a Bruker D8-Advance diffractometer with Cu-Kα radiation as the X-ray source. The molecular structures and functional groups of the obtained samples were identified using a Fourier Transform Infrared Spectrometer (FTIR) (Thermo Scientific Nicolet iS20) within the scan range 4000–400 cm^{-1}. UV-Vis diffuse reflectance spectra were performed on an Agilent Cary 5000 spectrophotometer. X-ray photoelectron spectroscopy (XPS) was carried out using the Thermo Scientific K-Alpha instrument with Al Kα radiation as the X-ray source. The elemental composition was determined using an Inductively Coupled Plasma Optical

Emission Spectrometer (ICP-OES) (Agilent 5800). N_2 adsorption-desorption experiments were performed using the BELSORP-Max automatic analyzer. The CO_2 adsorption experiments were measured using the Quanta AUTOSORB IQ automatic analyzer. The nitrogen content in the samples was analyzed using the Elementar vario Micro cube elemental analyzer.

Electrochemical measurement

The catalyst (10 mg) and carbon black (5 mg) were dispersed in 50 μL of a 5 wt% Nafion solution, 500 μL of ethanol and 500 μL of deionized water. The mixture was subjected to ultrasonic treatment for 30 minutes. Next, 50 μL of the homogenized catalyst ink was meticulously applied to a 1×1 cm^2 piece of SGL28BC hydrophobic carbon paper, after which the carbon paper was allowed to be dried.

The electrochemical experiment was conducted by an electrochemical workstation (DH7000) in an H-type electrolytic cell, which was divided into cathode and anode compartments by a Nafion117 proton exchange membrane. The CO_2RR was carried out in a three-electrode system, consisting of a working electrode, a counter electrode, and a reference electrode. The working electrode and the reference electrode (saturated calomel electrode) were placed in the cathode compartment, while the counter electrode (platinum mesh: 1 cm^2) was positioned in the anode compartment. The Linear Sweep Voltammetry (LSV) test was performed at a scanning frequency of 10 mV s^{-1}.

For the ECSA-normalized LSV curves, the specific capacitance for a flat surface typically ranges from 20 to 60 μF cm^{-2}. Therefore, we used a value of 40 μF cm^{-2} for our ECSA calculations.[1] The ECSA values for Co_0Zn_1-ZIF, $Co_{0.25}Zn_{0.75}$-ZIF, $Co_{0.5}Zn_{0.5}$-ZIF, $Co_{0.75}Zn_{0.25}$-ZIF and Co_1Zn_0-ZIF were 78, 92.5, 113.5, 176 and 46.5 cm^2, respectively.

Electrochemical impedance spectroscopy (EIS) was obtained by applying an AC voltage with an amplitude of 5 mV in the frequency range of 10^5 Hz to 0.1 Hz. Nyquist plots were obtained at 0 V and −0.65 V (vs. RHE). Cyclic voltammetry (CV) tests with different sweep speeds were performed in an Ar-saturated 0.5M $KHCO_3$ solution without the Faradaic process, and the double-layer capacitance was calculated after linear fitting. The gas product CO and H_2 generated during the CO_2RR process were detected using GC (Agilent 990). The liquid product was analyzed using Nuclear Magnetic Resonance spectroscopy (NMR) (Bruker AVANCE NEO 400M), with dimethyl sulfoxide (DMSO) employed as the internal standard. No liquid product was observed in this analysis. At 0.5 M $KHCO_3$ saturated with CO_2 (pH ≈ 7.2) and Ar (pH ≈ 8.8), the saturated calomel electrode (SCE) reference electrode was converted to a reversible hydrogen electrode (RHE) scale using the following equation: [2]

$$E\text{ (vs. RHE)} = E\text{ (vs. SCE)} + 0.222\text{ V} + 0.0592 \times \text{pH} \quad (1)$$

To evaluate the selectivity of the electrocatalysts, the Faradaic efficiency (FE) was calculated as follows: [3]

$$\text{FE}=\frac{N \times F \times n_{\text{p}}}{I_{\text{t}} \times t} \quad (2)$$

N represents the electron transfer number for a specific product, F represents the Faradaic constant (96485 C mol^{-1}), n_p represents the molars of product, I_t and t represent the total current and time, respectively.

TOF quantified the intrinsic electrical activity of the catalyst, the calculation formula was as follows: [2, 4]

$$\text{TOF (h}^{-1}\text{)}=\frac{j_{\text{product}}/NF}{m_{\text{catalyst}} \times \left(W_{\text{m}}/M_{\text{m}}\right)} \times 3600 \quad (3)$$

$j_{product}$ represents the product partial current density, N represents the electron transfer number for a specific product, F represents the Faradaic constant (96485 C mol^{-1}), $m_{catlyst}$ is the catalyst loading on the electrode, W_m is the metal loading in the catalyst, and M_m is the atomic mass of the metal.

Characterization

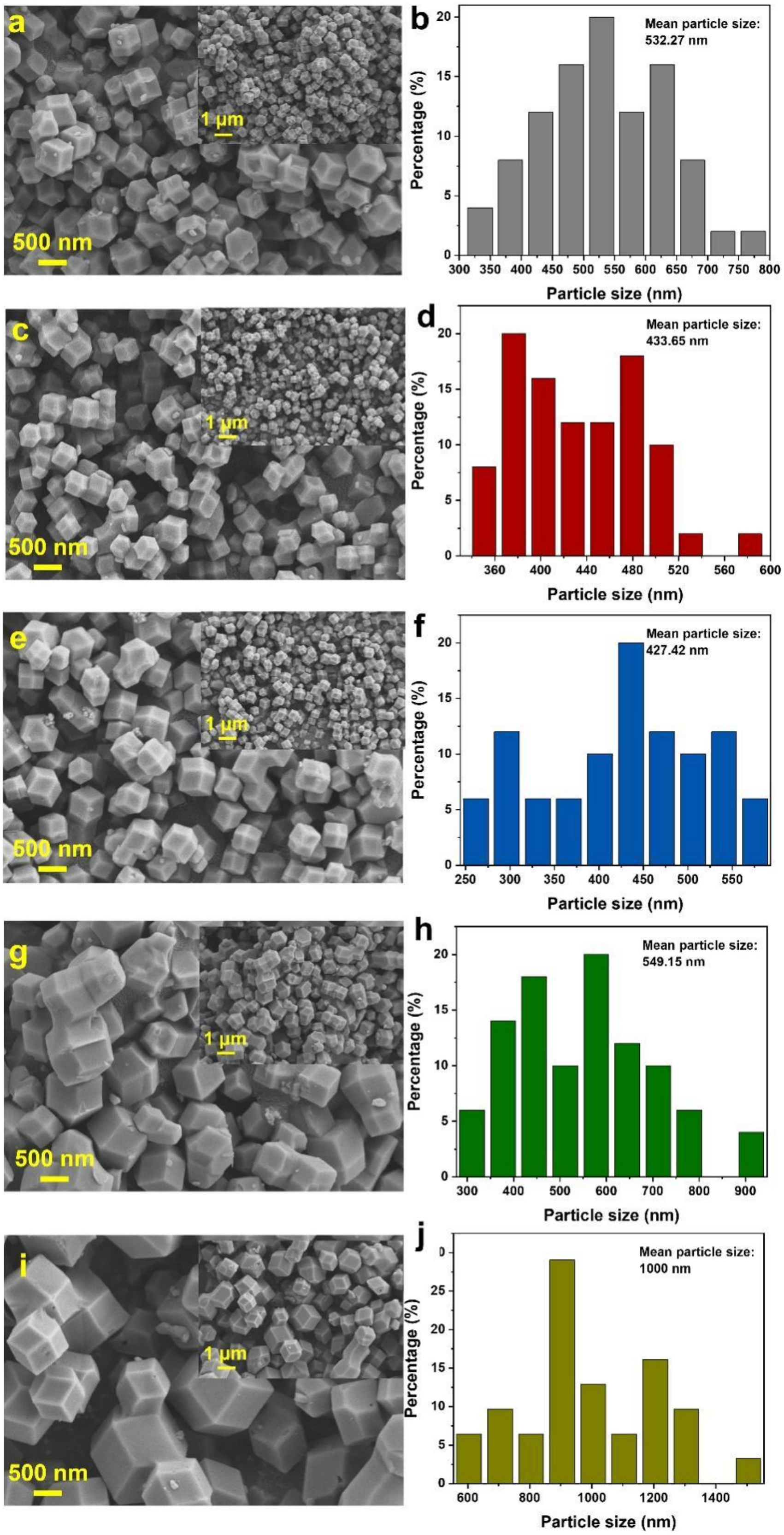

Fig. S1 SEM images and statistical graphs of particle sizes of (a and b) Co_0Zn_1-ZIF, (c and d) $Co_{0.25}Zn_{0.75}$-ZIF, (e and f) $Co_{0.5}Zn_{0.5}$-ZIF, (g and h) $Co_{0.75}Zn_{0.25}$-ZIF and (i and j) Co_1Zn_0-ZIF.

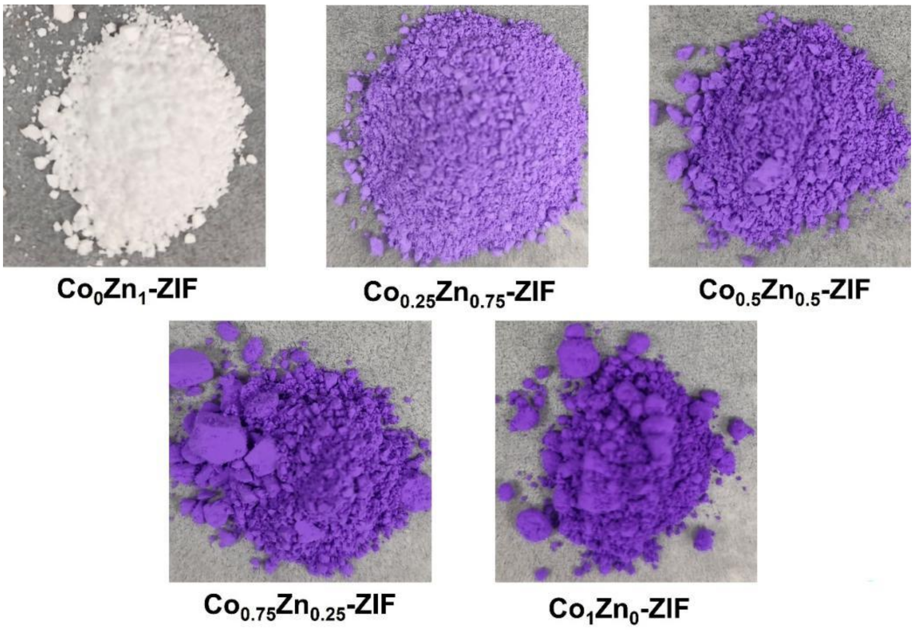

Fig. S2 Photos of Co_xZn_y-ZIF.

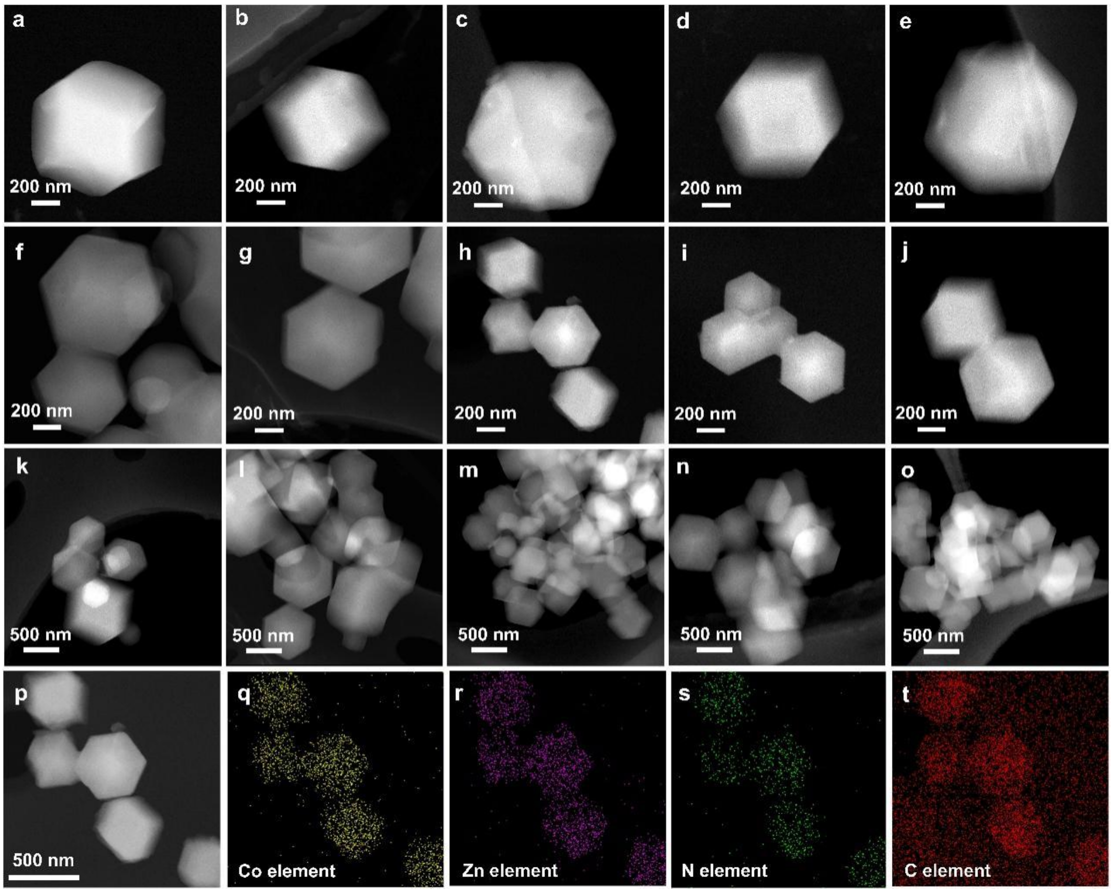

Fig. S3 STEM images Co_xZn_y-ZIF (a, f and k) Co_0Zn_1-ZIF, (b, g and l) $Co_{0.25}Zn_{0.75}$-ZIF, (c, h and m) $Co_{0.5}Zn_{0.5}$-ZIF, (d, i and n) $Co_{0.75}Zn_{0.25}$-ZIF, (e, j and o) Co_1Zn_0-ZIF and (p–t) EDS element distribution images of $Co_{0.5}Zn_{0.5}$-ZIF.

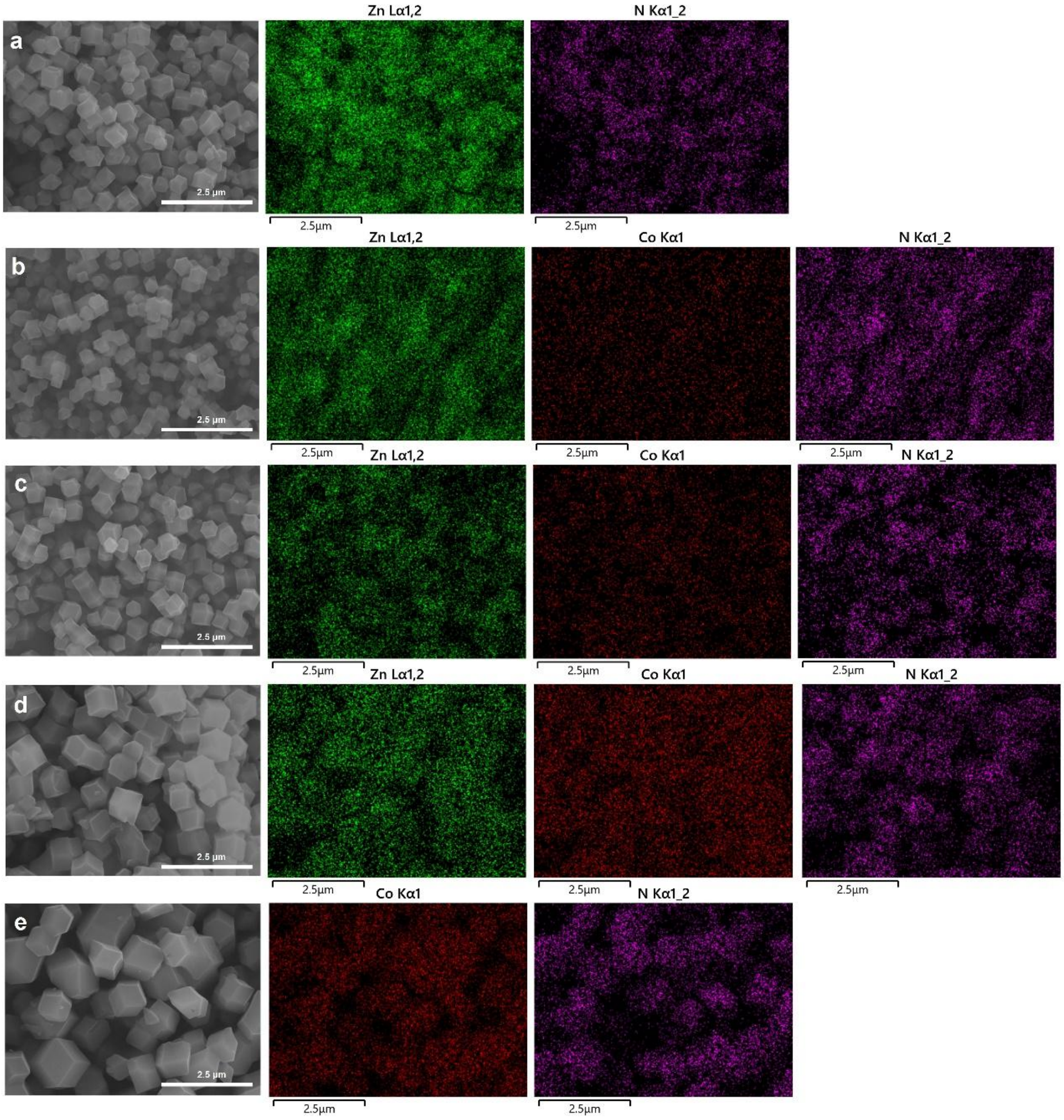

Fig. S4 SEM and EDS element distribution images of Co_xZn_y-ZIF (a) Co_0Zn_1-ZIF, (b) $Co_{0.25}Zn_{0.75}$-ZIF, (c) $Co_{0.5}Zn_{0.5}$-ZIF, (d) $Co_{0.75}Zn_{0.25}$-ZIF and (e) Co_1Zn_0-ZIF.

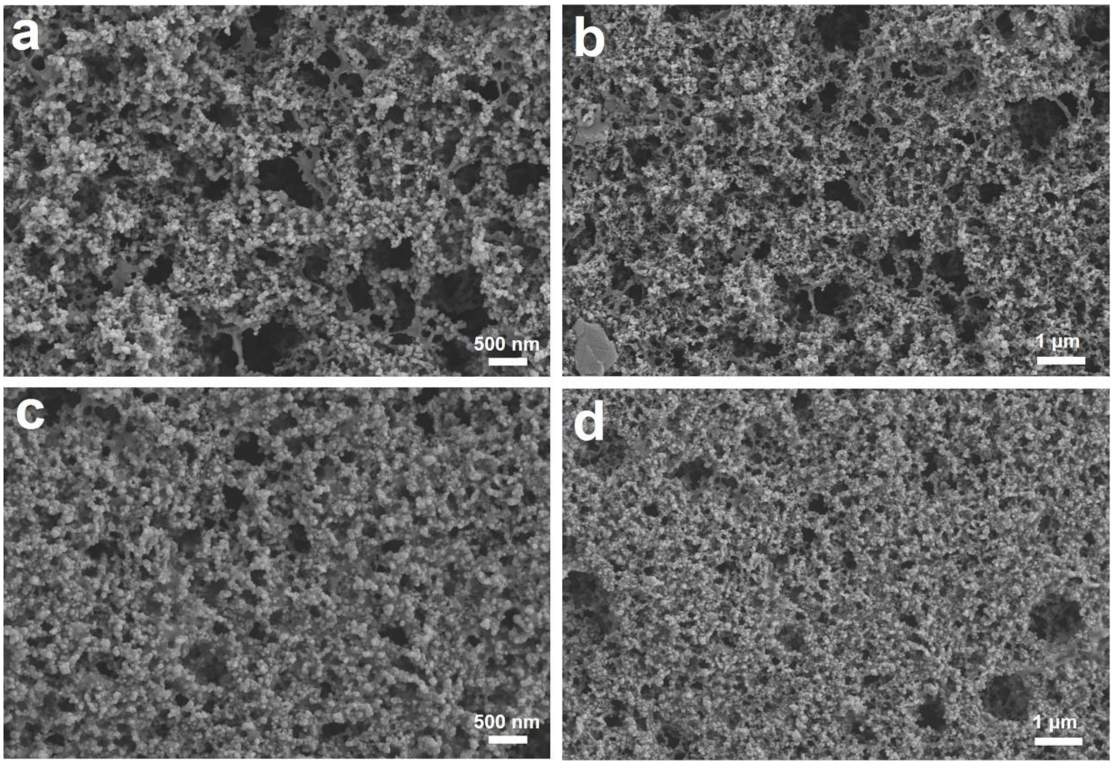

Fig. S5 SEM images of $Co_{0.5}Zn_{0.5}$-ZIF (a, b) after electrolysis at −1.3 V vs. RHE for 1.5 hours and (c, d) after electrolysis at −1.3 V vs. RHE for 10 hours.

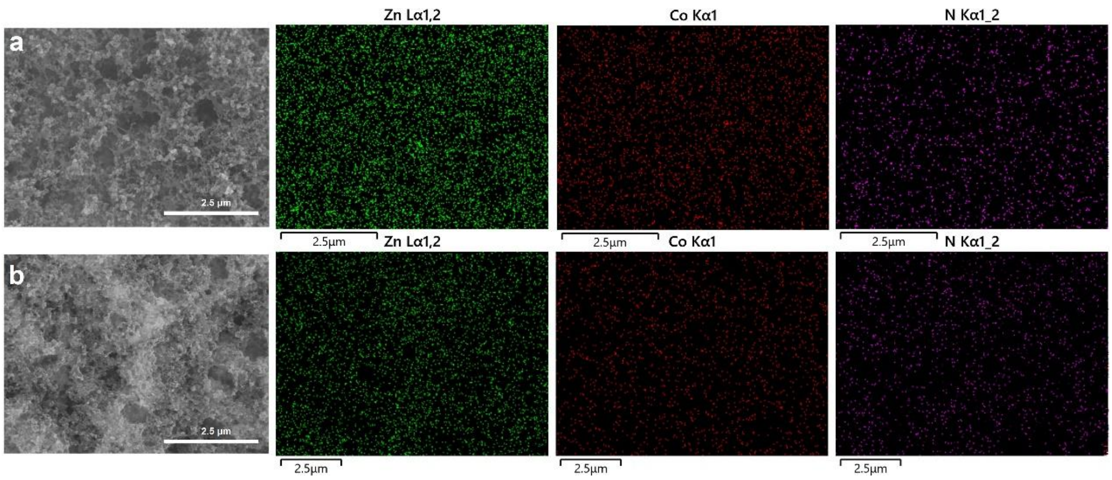

Fig. S6 SEM images and EDS element distribution of $Co_{0.5}Zn_{0.5}$-ZIF: (a) after electrolysis at −1.3 V vs. RHE for 1.5 hours and (b) after electrolysis at −1.3 V vs. RHE for 10 hours.

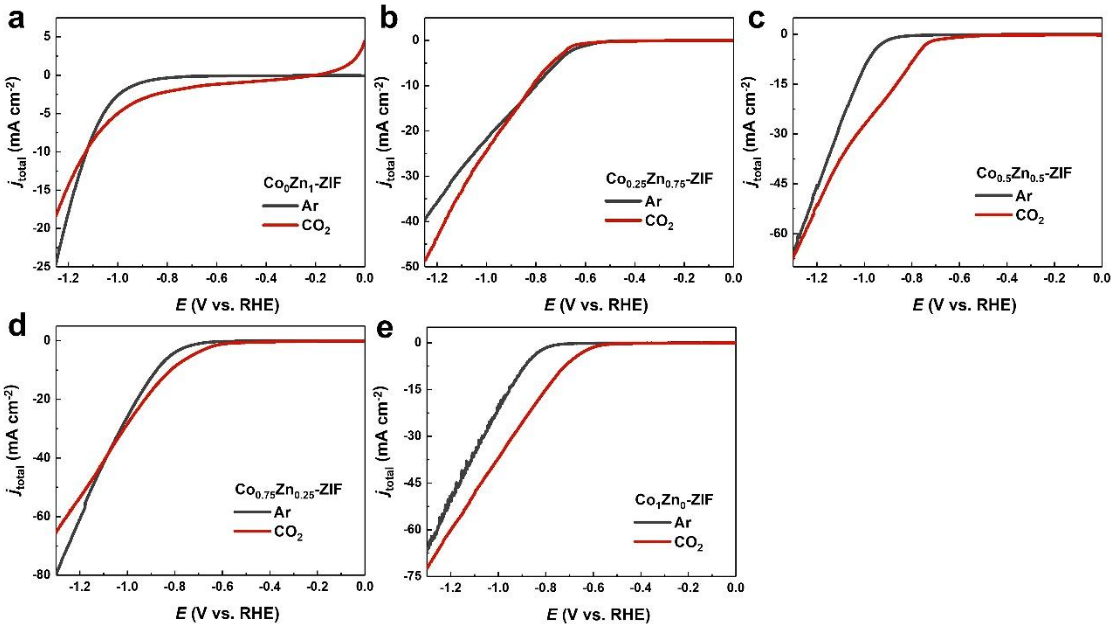

Fig. S7 LSV curves of Co_xZn_y-ZIF in 0.5 M $KHCO_3$ electrolyte purged by CO_2 and Ar.

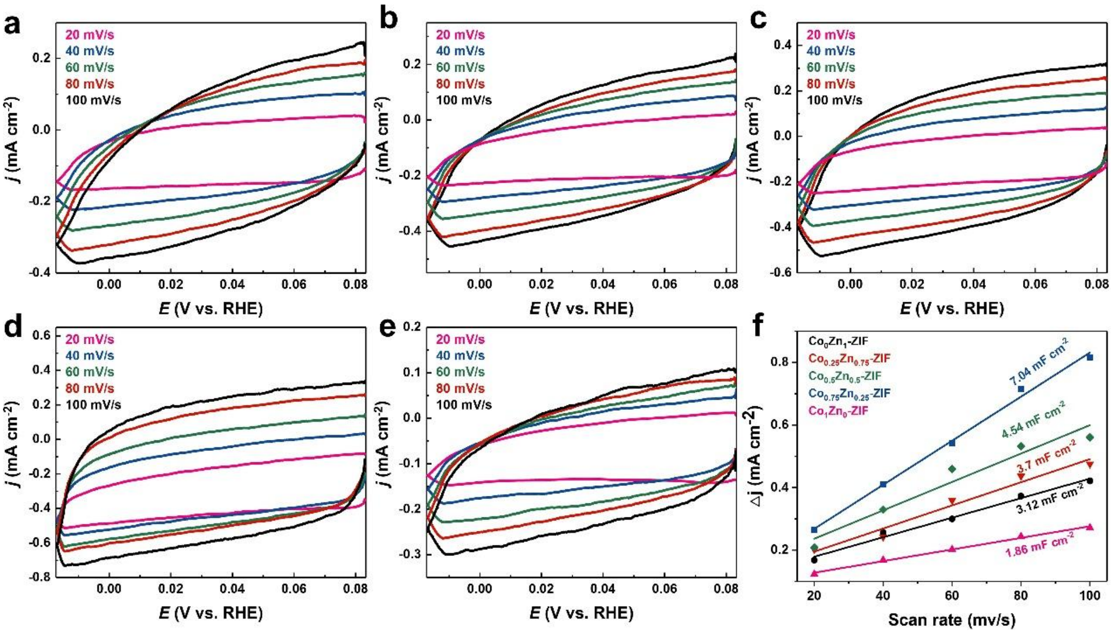

Fig. S8 CV plots of (a) Co_0Zn_1-ZIF, (b) $Co_{0.25}Zn_{0.75}$-ZIF, (c) $Co_{0.5}Zn_{0.5}$-ZIF, (d) $Co_{0.75}Zn_{0.25}$-ZIF, (e) Co_1Zn_0-ZIF and (f) C_{dl} values under different scanning rates.

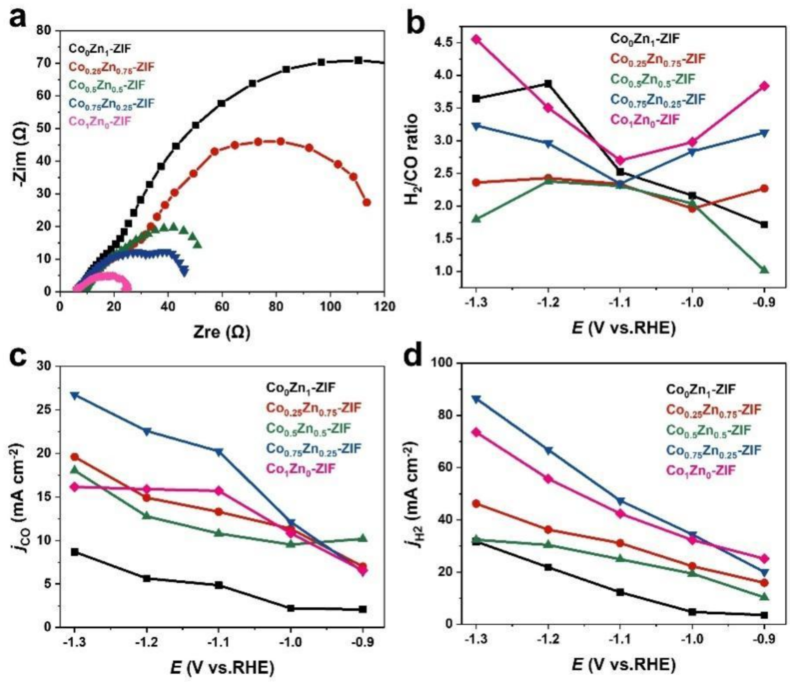

Fig. S9 (a) Nyquist curves (−0.65 V vs. RHE), (b) H_2/CO ratio, (c) j_{CO} and (d) j_{H2}.

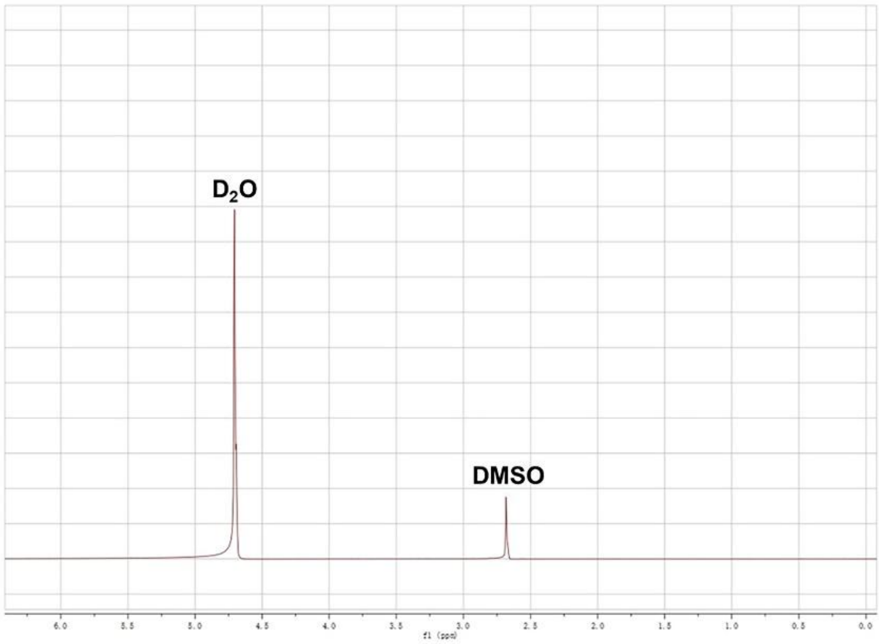

Fig. S10 ^{1}H NMR spectra of the electrolyte in the cathode chamber after electrolysis from −0.9 to −1.3 (V vs. RHE) for $Co_{0.5}Zn_{0.5}$-ZIF.

Table S1 ICP-AES data of Co_xZn_y-ZIF.

Catalyst	Zn (wt%)	Co (wt%)
Co_0Zn_1-ZIF	39.30	/
$Co_{0.25}Zn_{0.75}$-ZIF	25.47	6.77
$Co_{0.5}Zn_{0.5}$-ZIF	16.37	14.24
$Co_{0.75}Zn_{0.25}$-ZIF	7.98	20.19
Co_1Zn_0-ZIF	/	29.04

Table S2 EDS data of Co_xZn_y-ZIF.

Catalyst	Zn (wt%)	Co (wt%)	N (wt%)	C (wt%)
Co_0Zn_1-ZIF	11.4	/	23.74	64.86
$Co_{0.25}Zn_{0.75}$-ZIF	5.28	1.35	21.13	72.23
$Co_{0.5}Zn_{0.5}$-ZIF	4.00	3.54	22.07	70.38
$Co_{0.75}Zn_{0.25}$-ZIF	3.94	9.66	26.30	60.10
Co_1Zn_0-ZIF	/	11.93	26.56	61.51

Table S3 The N content of Co_xZn_y-ZIF.

Catalyst	N (wt%)
Co_0Zn_1-ZIF	24.24
$Co_{0.25}Zn_{0.75}$-ZIF	24.68
$Co_{0.5}Zn_{0.5}$-ZIF	24.55
$Co_{0.75}Zn_{0.25}$-ZIF	25.08
Co_1Zn_0-ZIF	24.91

Table S4 Comparison of the performance of the catalysts in this work with that of the reported excellent literature on syngas production.

Catalyst	Electrolyte	Cell type	*E* (V vs. RHE)	H_2/CO ratio	*E* (V vs. RHE)	j_{total} (mA cm^{-2})	Ref.
			ZIFs-based MOFs				
$Co_{0.5}Zn_{0.5}$-ZIF	0.5 M $KHCO_3$	H type	−0.9	1.0	−0.9	−26	This work
$Co_{0.25}Zn_{0.75}$-ZIF	0.5 M $KHCO_3$	H type	−1	2.0	/	/	This work
$Co_{0.75}Zn_{0.75}$-ZIF	0.5 M $KHCO_3$	H type	−1.2	3.0	/	/	This

							work
10%Ag-ZIF-8	0.5 M $KHCO_3$	H type	−1.1	0.4	−1.1	−2.6	5
10%Ag-ZIF-8	1M KOH	H type	−0.9	0.3	−0.9	−28	5
F-Cu_2O@ZIF-8	0.1M $KHCO_3$	H type	−0.7	2.0	−0.7	−1.25	6
F-Cu_2O@ZIF-8	0.1 M $KHCO_3$	H type	−0.9	0.2	−0.9	−6.25	6
F-Cu_2O@ZIF-8	0.1 M $KHCO_3$	H type	−1.0	0.2	−1.3	−17	6
Cu_{ZIF}	/	/	−1.5	0.5	−1.5	−0.8	7
			ZIF-derived SACs				
Co-HNC	0.1 M $KHCO_3$	/	−0.9	2.0	−1.4	−25	8
Co-HNC	0.1 M $KHCO_3$	/	−1.0	2.0	/	/	8
C-Fe-Co-ZIF 1.6 wt% Fe	0.5 M $KHCO_3$	H type	−0.8	3.4	/	/	9
C–Co–ZIF HM 15min	0.5 M $KHCO_3$	H type	−0.8	2.3	/	/	10
C–Co–ZIF HM 15min	0.5 M $KHCO_3$	H type	−0.7	1.0	/	/	10
FeN_4C	0.1 M $KHCO_3$	H type	−0.8	2.5	/	/	11
			Other SACs				
Ni−Fe DASs (3:1)	0.5 M $KHCO_3$	/	−1.1	1.0	−0.7	−20	12
Ni−Fe DASs (2:2)	0.5 M $KHCO_3$	/	−1.1	0.5	−0.7	−20	12
Ni−Fe DASs (1:3)	0.5 M $KHCO_3$	/	−1.1	3.1	/	/	12
Ni, Fe-hG	0.1 M $KHCO_3$	H type	−0.6 to −1.1	1.0	/	/	13
Ni-hG/Fe-hG	0.1 M $KHCO_3$	H type	−0.6 to −1.1	1.0	/	/	13
Ni-hG/Fe-hG	0.1 M $KHCO_3$	Com'l	2.5	3	2.5	55	13
			ZIF-derived materials				
10-Co_2L@ZIF-8-850	0.1 M $KHCO_3$	H type	−1.0	2.0	−0.8	20	14
10-Co_2L@ZIF-8-850	0.1 M $KHCO_3$	H type	/	/	−1.0	31.7	14
Cu_{ZIF}-500	/	/	−1.1	3.0	−1.5	0.75	7
Cu_{ZIF}-500	/	/	−1.3	2.0	−1.5	0.75	7
Cu_{ZIF}-500	/	/	−1.5	1.0	−1.5	0.75	7
Cu_{ZIF}-700	/	/	−1.1	4.0	−1.5	0.25	7
Cu_{ZIF}-700	/	/	−1.5	2.0	/	/	7
Cu_{ZIF}-900	/	/	−1.5	3.0	−1.5	3.0	7

Fe/FeN$_4$C	0.1 M $KHCO_3$	H type	−0.8	7.1	−0.8	39.33	11
			Other materials				
UNCNs-900	0.1 M $KHCO_3$	H type	−0.9	1.0	−0.9	3.0	15
UNCNs-900	0.1 M $KHCO_3$	H type	−1.1	2.0	−1.1	7.5	15
10 nm Au	0.5 M $KHCO_3$	H type	−0.9	3.0	/	/	16
8 nm Au	0.5 M $KHCO_3$	H type	−0.9	9.0	−0.87	17.5	16

References

[1] T. Wang, Q. Zhang, K. Lian, G. Qi, Q. Liu, L. Feng, G. Hu, J. Luo and X. Liu, *J. Colloid Interface Sci.*, 2024, **655**, 176–186.

[2] J. H. Cho, C. Lee, S. H. Hong, H. Y. Jang, S. Back, M. g. Seo, M. Lee, H. K. Min, Y. Choi and Y. J. Jang, *Adv. Mater.*, 2022, **35**, 2208224.

[3] F. Lyu, W. Hua, H. Wu, H. Sun, Z. Deng and Y. Peng, *Chin. J. Catal.*, 2022, **43**, 1417–1432.

[4] S. Liang, T. Zhang, Y. Zheng, T. Xue, Z. Wang, Q. Wang and H. He, *Appl. Catal., B*, 2023, **333**, 122801.

[5] M. Usman and M. H. Suliman, *Catalysts*, 2023, **13**, 867.

[6] H. Luo, B. Li, J. G. Ma and P. Cheng, *Angew. Chem. Int. Ed.*, 2022, **61**, e202116736.

[7] S. Cui, C. Yu, X. Tan, H. Huang, X. Yao and J. Qiu, *ACS Sustainable Chem. Eng.*, 2020, **8**, 3328–3335.

[8] X. Song, H. Zhang, Y. Yang, B. Zhang, M. Zuo, X. Cao, J. Sun, C. Lin, X. Li and Z. Jiang, *Adv. Sci.*, 2018, **5**, 1800177.

[9] Z. Chen, G. Zhang, Y. Wen, N. Chen, W. Chen, T. Regier, J. Dynes, Y. Zheng and S. Sun, *Nano-Micro Lett.*, 2022, **14**, 25.

[10] Z. Chen, G. Zhang, Q. Hu, Y. Zheng, S. Cao, G. Chen, C. Li, T. Boyko, N. Chen and W. Chen, *Small Struct.*, 2022, **3**, 2200031.

[11] Y. Hua, B. Zhang, W. Hao and Z. Gao, *Cell Rep. Phys. Sci.*, 2022, **3**, 100703.

[12] L. Wang, X. Gao, S. Wang, C. Chen, J. Song, X. Ma, T. Yao, H. Zhou and Y. Wu, *J. Am. Chem. Soc.*, 2023, **145**, 13462–13468.

[13] J. Leverett, R. Daiyan, L. Gong, K. Iputera, Z. Tong, J. Qu, Z. Ma, Q. Zhang, S. Cheong and J. Cairney, *ACS Nano*, 2021, **15**, 12006–12018.

[14] W. Yang, J.-H. Zhang, R. Si, L.-M. Cao, D.-C. Zhong and T.-B. Lu, *Inorg. Chem. Front.*, 2021, **8**, 1695–1701.

[15] B. Wei, J. Hao, B. Ge, W. Luo, Y. Chen, Y. Xiong, L. Li and W. Shi, *J. Colloid Interface Sci.*, 2022, **608**, 2650–2659.

[16] W. Zhu, R. Michalsky, O. n. Metin, H. Lv, S. Guo, C. J. Wright, X. Sun, A. A. Peterson and S. Sun, *J. Am. Chem. Soc.*, 2013, **135**, 16833–16836.